LITERATURE CITED

Bird, R. B., W. E. Stewart, and E. N. Lightfoot, *Transport Phenomena*, Wiley, New York (1960).

Dribika, M. M., "Simultaneous Heat and Mass Transfer for Multicomponent Distillation in a Wetted-Wall Column," M. S. Thesis, Univ. of California, Santa Barbara (1977).

Dribika, M. M., and O. C. Sandall, "Simultaneous Heat and Mass Transfer for Multicomponent Distillation in a Wetted-Wall Column," *Chem. Eng. Sci.*, **34**, 733 (1979).

Free, K. W., and H. P. Hutchison, "Three Component Distillation at Total Reflux," *Proc. Int. Symp. Distillation*, Brighton, England (1960).

Gmehling, J., and U. Onken, *Vapor-Liquid Equilibrium Data Collection*, **1**, pt. 1, DECHEMA, Frankfurt (1977).

Johnstone, H. F., and R. L. Pigford, "Distillation in a Wetted-Wall Column," *Trans. AIChE*, **38**, 25 (1942).

Krishna, R., "A Simplified Mass Transfer Analysis for Multicomponent Condensation," *Letters, Heat & Mass Transfer*, **6**, 439 (1979).

Krishna, R., H. F. Martinez, R. Sreedhar, and G. L. Standart, "Murphree Point Efficiencies in Multicomponent Systems," *Trans. Inst. Chem. Engrs.*, **55**, 178 (1977).

Krishna, R., and G. L. Standart, "A Multicomponent Film Model Incorporating a General Matrix Method of Solution to the Maxwell-Stefan Equations," *AIChE J.*, **22**, 383 (1976).

Krishna, R., and G. L. Standart, "Mass and Energy Transfer in Multicomponent Systems," *Chem. Eng. Commun.*, **3**, 201 (1979).

Nord, M., "Plate Efficiencies of Benzene-Toluene-Xylene Systems in Distillation," *Trans. Inst. Chem. Engrs.*, **42**, 863 (1946).

Prausnitz, J., T. Anderson, E. Grens, C. Eckert, R. Hsieh, and J. P. O'Connell, *Computer Calculations for Multicomponent Vapor-Liquid and Liquid-Liquid Equilibria*, Prentice-Hall, Englewood Cliffs, NJ (1980).

Reid, R. C., J. M. Prausnitz, and T. K. Sherwood, *The Properties of Gases and Liquids*, 3rd ed., McGraw-Hill, New York (1977).

Sherwood, T. K., R. L. Pigford, and C. R. Wilke, *Mass Transfer*, McGraw-Hill, New York (1975).

Smith, L. W., and R. Taylor, "Film Models for Multicomponent Mass Transfer: A Statistical Comparison," *Ind. Eng. Chem. Fund.*, **22**, 97 (1983).

Stewart, W. E., and R. Prober, "Matrix Calculation of Multicomponent Mass Transfer in Isothermal Systems," *Ind. Eng. Chem. Fund.*, **3**, 224 (1964).

Taylor, R., and L. W. Smith, "On Some Explicit Approximate Solutions of the Maxwell-Stefan Equations for the Multicomponent Film Model," *Chem. Eng. Commun.*, **14**, 361 (1982).

Toor, H. L., "Solution of the Linearized Equations of Multicomponent Mass Transfer, *AIChE J.*, **10**, 448, 460 (1964).

Vogelpohl, A., "Murphree Efficiencies in Multicomponent Systems, *Ind. Chem. Eng. Symp. Ser.*, **2**(1), 25 (1979).

Manuscript received July 29, 1983, and accepted Jan. 28, 1984.

A Novel Radioactive Particle Tracking Facility for Measurement of Solids Motion in Gas Fluidized Beds

J. S. LIN, M. M. CHEN, and B. T. CHAO

Department of Mechanical and Industrial Engineering
University of Illinois
Urbana, IL 61801

Measurements of solids motion in a fluidized bed have been made in a computer-aided particle tracking facility. A radioactive tracer particle, dynamically identical to the solid particles to be studied, was mixed with the solids in the bed. The gamma radiation from the tracer was continuously monitored by a large number of scintillation detectors located around the bed, providing information on the tracer's instantaneous location. Prudent use was made of the purposely introduced redundant distance data to achieve improved accuracy. The recognition of the existence of secondary emission due to the interaction of the primary radiation and other system materials and the subsequent devising of a scheme to mitigate its effect contribute much to the success. Results for a bed with a uniform air distributor plate show the existence of two counter-rotating toroidal vortices whose relative sizes and strengths vary with the fluidizing velocity. Fluctuating motions at low frequencies ranging from 1.6 to 16 Hz have been observed at various locations in the bed.

SCOPE

Solids motion plays important roles in various applications of fluidized bed technology. Among these applications are the enhancement of heat and mass transfer, material processing, catalytic cracking, particle sedimentation, and others. A better understanding of solids movement is often crucial to the fulfillment of the promise of these fluidization applications and to the further development of fundamental fluidization theories. Despite its importance, there is little information on particle motion in fluidized beds. Quantitative, comprehensive data for solids velocity distribution are lacking. Those reported in the open literature are often qualitative, incomplete, or inconsistent.

Correspondence concerning this paper should be addressed to J. S. Lin, who is presently with Allied Corp., Parsippany, NJ 07054.

A major reason for the present unsatisfactory state in this regard is that the opacity of particles and their interference with a probe placed in the bed have severely hampered the development of successful measuring techniques.

The objectives of the present research are to develop a facility to study solids motion and to obtain detailed information on solids dynamics, such as mean velocity distributions and correlations of fluctuating velocities, in a three-dimensional gas fluidized bed under various operating conditions. To this end, a computer-aided particle tracking facility was built. The measuring technique is based on the continuous tracking of a radioactive tracer particle which is dynamically identical to the particle species in the bed under study. As the tracer particle moves in the bed, its gamma radiation is continuously monitored by twelve scintillation detectors located around the bed. The count rate at each detector is interpreted by a computer to yield the distance between the tracer and that detector, using a previously established calibration. The computer then proceeds to determine the instantaneous location of the tracer by triangulation from twelve distances. Since these are more than the required minimum of four distances, the redundancy is utilized to improve accuracy by reducing the influence of intrinsic noise associated with the quantized nature of gamma emission. The displacements are then time-differentiated to yield instantaneous velocities. Ensemble-averaged velocities of solids and other statistical quantities are obtained from a large number of such data gathered over a period of several hours.

Measurements of mean velocity distribution were made for glass beads of density 2.5 g/cm^3 and diameters ranging from 0.42 to 0.8 mm in an air fluidized bed of 13.8 cm diameter, at various fluidizing velocities ranging from 1.6 to 4.6 times the minimum fluidization velocity. Sample measurements under a limited range of conditions were also made for a bed with a distributor plate smaller than the bed cross section and for a bed with an immersed sphere. In an attempt to elucidate the dynamics of particle motion, Lagrangian autocorrelations for both axial and radial fluctuating velocities were calculated.

CONCLUSIONS AND SIGNIFICANCE

The following conclusions are based on results obtained under conditions within the limits of the present investigation.

1. A particle tracking facility for measuring solids motion in air fluidized beds has been developed. To our knowledge the present undertaking is the first successful attempt by which detailed quantitative information on solids velocities in a fluidized bed has been obtained. An innovation of the experimental scheme is to take full advantage of deliberately introduced high redundancy in location determination of the tracer particle. The recognition of the effect of secondary emission due to the interaction of the primary radiation and system materials, and the devising of a scheme for alleviating this effect also contribute to the success.

2. The fluidizing velocity and the distributor plate configuration have a dominating influence on the solids circulation pattern. With a uniform distributor plate and at low air velocities, the solids motion is characterized by a single toroidal vortex with particles ascending near the wall and descending in the central region of a cylindrical bed (AWDC). With increasing air velocity, a second toroidal vortex in the opposite direction (ascending in center, descending near wall—ACDW) appears in the upper region of the bed. Further increases in air velocity promote the increasing dominance of the ACDW vortex at the expense of the AWDC vortex in the lower region. At sufficiently high velocities, the AWDC vortex disappears. When the air velocity is such that the two opposing vortices coexist, there is a layer of negligibly small vertical velocity that separates the two vortices. Occasionally, this layer can be observed visually as a stagnant ring on the interior surface of the transparent bed wall. Restricting the air flow to the central core of the distributor plate greatly enhances the ACDW vortex and may completely suppress the AWDC circulation. The presence of an immersed sphere of diameter approximately $^2/_5$ of the bed diameter reduces significantly the solids circulation rate. The particle tracking facility is able to reveal the stagnant region at the top of the sphere.

3. When two opposing vortices coexist, the Lagrangian autocorrelation coefficient for the axial motion indicates a relatively high frequency (about 16 Hz) region at the vicinity of the distributor plate. As one moves away from the plate, this characteristic frequency decreases and reaches a minimum (about 1.6 Hz) in the layer that separates the two opposing vortices. The solids above this imaginary layer again exhibit a higher frequency. The Lagrangian autocorrelation coefficient for the radial component of the solids velocity, unlike that for the axial motion, is remarkably insensitive to locations in the bed. This observation is unexplained at the present time.

The behavior of solids motion revealed in the present study should be useful to enhance the development of the fluid mechanical theories of fluidized beds. It is also useful to the practicing engineer. The particle tracking facility promises to be a valuable tool for the rational design of fluidized beds.

INTRODUCTION

The recirculation pattern with particles ascending at the center and descending near the wall (ACDW) was reported in small beds (Leva, 1962; Marsheck and Gomezplata, 1965). The reversed pattern, i.e., ascending near the wall and descending at the center (AWDC), was observed for a shallow bed by Ohki and Shirai (1975) and for large beds by Whitehead et al. (1976). Based on measurements of the bubble motion, Werther and Molerus (1973) speculated that depending on the fluidization velocity and the bed height-to-diameter ratio, both patterns of ACDW and AWDC could coexist in a gas fluidized bed.

Among the existing quantitative measuring techniques, perhaps the most direct methods to study particle motion are individual particle tracing techniques. Cinematography has been commonly used for transparent liquid fluidized beds, where the refractive index of particles is closely matched with that of the fluidizing liquid to track the individual darkened tracer (Handley et al., 1966; Carlos and Richardson, 1968; Latif and Richardson, 1972; Kmiec, 1978). Unfortunately, these techniques are too laborious to obtain statistically meaningful velocity distributions. Some are of doubtful practical interest since the solids studied are too large relative to the bed size, e.g., 6–8 mm particles in 5–10 cm beds (Carlos and Richardson, 1968; Latif and Richardson, 1972; Kmiec 1978). For gas fluidized beds, Massimilla and Westwater (1960) cinematographically obtained particle trajectories at the wall. Subsequently, other investigators attempted to probe the motions of the interior particles. Merry and Davidson (1973) used a 20 mm-diameter "radio pill" containing a transmitter to measure particle velocities at the center of a shallow bed fluidized by an uneven air flow to form the so-called "gulf stream." The disadvantage of the method is that the motion of the very large tracer can hardly be represen-

tative of the bed particles. The presence of a bulky radio receiver in the form of an aerial network placed in the bed might also severely disturb the flow patterns. More recently, Ohki et al. (1975, 1977, 1980) developed optical fiber probes to measure particle velocities. The technique shares the same drawback as many others in that the measuring probe could interfere with the solids and bubble activities. To eliminate the problem of flow disturbance, Kondukov et al. (1964) and Velzen et al. (1974) employed radioactive particle tracking methods. Unfortunately, only sketchy qualitative information was reported, presumably due to the lack of adequate instrumentation and sufficiently comprehensive data reduction schemes.

In the present investigation, considerable effort was made to develop an efficient photon-counting instrumentation by making use of the relationship between gamma ray intensity and the particle-to-detector distance. Full advantage was taken of data redundancy, which was deliberately introduced by installing a large number of scintillation detectors around the bed. These efforts contributed to the success of the present experimentation.

COMPUTER-AIDED PARTICLE TRACKING FACILITY

Hardware Development

The tracer particle was made of scandium-46 and was closely matched to the size and density of the glass beads used as fluidized particles. Scandium-46 was selected for the following reasons: (1) It has a specific gravity of 2.89 which is only slightly greater than that of the glass beads. Hence, only a very small amount of nonradioactive material needs to be added to match the density. This results in a tracer of high radioactivity. (2) It emits gamma rays at 0.89 Mev and 1.12 Mev. The energy range is such that the mass absorption coefficient is relatively independent of most absorbing materials. (3) It has a relatively high specific activity and moderate half life (84 days), making the activation of the tracer in a reactor reasonably convenient. Two different sizes of scandium ball coated with epoxy were used in the experiments, the finished diameters being 0.7 mm and 0.5 mm, respectively. Experiments indicated that radioactivity of 100~150 microcuries was adequate, yielding approximately 50,000 counts/s when the tracer was at the center of the empty bed of 14 cm diameter.

Twelve photomultiplier tubes (PMT) incorporating Bicron 2 in.

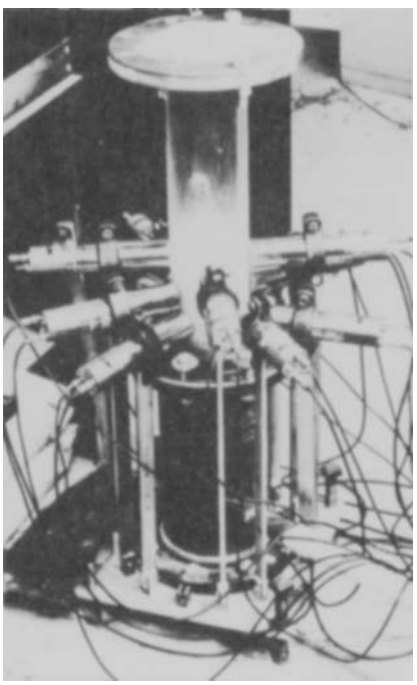

Figure 1. Twelve scintillation detectors surrounding a gas fluidized bed.

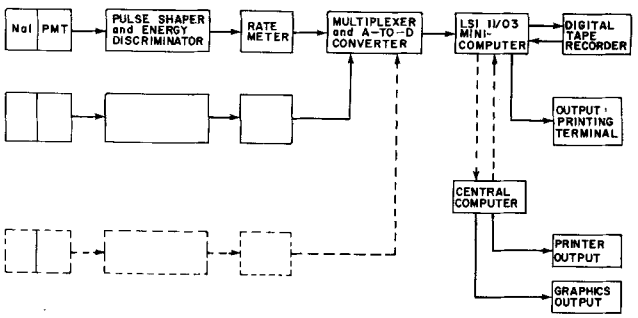

Figure 2. Schematic diagram of photon counting devices and data acquisition system.

× 2 in. (5.08 cm × 5.08 cm) sodium iodide (NaI) crystals were used to continuously monitor the gamma ray emission from the tracer. As shown in Figure 1, the twelve detectors were arranged in a staggered configuration at three different heights, with four in each level. This arrangement offers the advantage that wherever the tracer is, there are several detectors nearby, thus providing accurate distance measurements. As the tracer moves around the bed, twelve intensity measurements are made by the detectors at any time, giving the "instantaneous" position of the tracer. A data reduction scheme for determining the tracer location from the intensity measurements is discussed later. Additional detectors could be installed to improve resolution or to study solids motion in deeper beds.

The photon counting scheme and the data acquisition system are shown schematically in Figure 2. Details of the electronic circuitry can be found in Lin (1981). The raw signals have a noisy background mainly originating from secondary emissions due to the interaction of gamma rays with bed materials. Since the secondary emissions are essentially of fairly low energies, their effect can be effectively removed by employing a Schmitt trigger with an adjustable threshold. In order to determine the optimal threshold voltage for the Schmitt trigger, the spectral energy distribution of the Sc-46 tracer as seen by one of the PMT's was obtained by using a single channel analyzer. A typical result is shown in Figure 3. The dashed line is for an empty bed while the solid line is for a bed in the presence of particles. The two distinct peaks of 0.89 Mev and 1.12 Mev are clearly due to the primary emissions of Sc-46. It is seen that the presence of particles contributed significantly to the low energy end of the spectrum at the expense of the small number of photons possessing higher energy. The trend remained the same for other locations of the tracer (Lin, 1981). Therefore, it was concluded that a threshold voltage between 3 and 4 volts would eliminate the extraneous contributions of secondary emissions for all practical purposes. The recognition of the presence of secondary emissions and the use of appropriate energy-discriminating circuitry to circumvent their effects are crucial in obtaining useful results in this investigation.

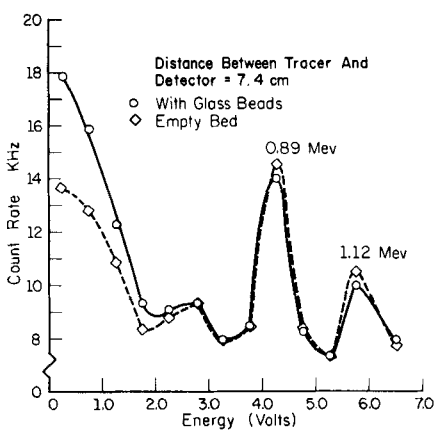

Figure 3. Effect of secondary emission due to the presence of particles.

The measured count rates were then fed into a microcomputer-based data acquisition system via a multiplexer.

Establishment of Distance-Intensity Relationship

A monotonic relationship between intensity (i.e., count rate) and distance of the tracer to each detector was established by calibration. The density dependence of gamma ray attenuation through the bed makes it necessary to calibrate in situ because of the inhomogeneity of the bubbling fluidized bed. Of particular concern was whether this relationship would vary with the angle from the axis of the cylindrical detector. As it turned out, an empirical center of an NaI crystal near the geometrical center of the crystal could be found, with the result that angular dependence was virtually eliminated (Lin, 1981). Thus, a single calibration curve relating intensity to distance can be established for each detector. A typical curve is shown in Figure 4. Hence, our intensity measurement is tantamount to a distance measurement. For the convenience of data reduction, all calibration curves were fitted to a third degree polynomial of the following form:

$$r_i = f(1/I_i) = a_{0i} + a_{1i}(1/I_i) + a_{2i}(1/I_i)^2 + a_{3i}(1/I_i)^3 \quad (1)$$

where r_i and I_i denote distance and intensity associated with the ith detector; a_{0i}, a_{1i}, etc., are coefficients determined by a least-square method.

Clearly, the closer the tracer is to the detector, the better the measurement resolution is. Recognition of this fact leads to the use of a large number of detectors as previously discussed. Furthermore, a weighted linear regression scheme of data processing was used, placing heavier weight on data originating from higher intensities.

Data Reduction Scheme for Determining Tracer Location

The availability of distance measurements from 12 scintillation detectors resulted in data redundancy for location determination. To take advantage of this planned redundancy, a weighted least-square method based on an exact linearization scheme was used.

The distance between the tracer and the ith detector is given by

$$(\xi - x_i)^2 + (\eta - y_i)^2 + (\zeta - z_i)^2 = r_i^2 \quad (2a)$$

where ξ, η, ζ denote the coordinates of the tracer to be determined, x_i, y_i, z_i denote coordinates of the effective fictitious center of the ith crystal as described previously, r_i is its distance to the tracer, and $i = 1,2,\ldots n$, n being the total number of detectors used. Physically, Eq. 2a implies that associated with each detector there is an imaginary sphere centered at (x_i,y_i,z_i) of radius r_i with the tracer at (ξ,η,ζ) on the surface of the sphere. Thus (ξ,η,ζ) can always be determined uniquely by four equations, employing one of them to resolve the ambiguity of multiple solutions if only three equations were used. However, the solutions obtained by solving any set of four equations out of n equations vary, because of the inherent fluctuation of gamma ray count rate and the changing attenuation, however small, due to random motion of bubbles in the bed. In an effort to obtain an efficient algorithm to determine the optimum solution, a weighted linear regression method was developed. Rearranging terms in Eq. 2a, we obtain:

$$\mu - 2\xi x_i - 2\eta y_i - 2\zeta z_i = r_i^2 - x_i^2 - y_i^2 - z_i^2 \quad (2b)$$

where $\mu \equiv \xi^2 + \eta^2 + \zeta^2$ and hereafter will be treated as a separate unknown. In this way, the equation set 2a is linearized. Rewriting Eq. 2b in matrix form, we have,

$$|X|\,|\beta| = |Z| \quad (3)$$

in which

$$|X| = \begin{bmatrix} 1 & -2x_1 & -2y_1 & -2z_1 \\ 1 & -2x_2 & -2y_2 & -2z_2 \\ \cdot & \cdot & \cdot & \cdot \\ \cdot & \cdot & \cdot & \cdot \\ \cdot & \cdot & \cdot & \cdot \\ 1 & -2x_n & -2y_n & -2z_n \end{bmatrix}_{n\times 4} \quad (3a)$$

$$|\beta| = \begin{bmatrix} \mu \\ \xi \\ \eta \\ \zeta \end{bmatrix}_{4\times 1} \quad (3b)$$

and

$$|Z| = \begin{bmatrix} r_1^2 - x_1^2 - y_1^2 - z_1^2 \\ r_2^2 - x_2^2 - y_2^2 - z_2^2 \\ \vdots \\ r_n^2 - x_n^2 - y_n^2 - z_n^2 \end{bmatrix}_{n\times 1} \quad (3c)$$

It is noted that $|X|$, a hardware constant, depends only on the coordinates of the fictitious centers of the n detectors; $|\beta|$ consists of the instantaneous coordinates of the tracer; and $|Z|$ is determined by the observed distances from each detector. Since errors in the measurements of $r_1,r_2\ldots r_n$ invariably exist, Eq. 3 is modified to become:

$$|Z| = |X|\,|\beta| + |E| \quad (4)$$

where

$$|E| = \begin{bmatrix} \epsilon_1 \\ \epsilon_2 \\ \vdots \\ \epsilon_n \end{bmatrix}_{n\times 1} \quad (4a)$$

which is the error vector for the estimation of $|\beta|$.

As has been pointed out previously, the distance measurements by the detectors are not equally accurate. The closer the tracer is to the detector, the better is the signal-to-noise ratio. Therefore in order to obtain an optimal solution for $|\beta|$, appropriate weighting functions are introduced. To this end, use is made of linear regression theory and Eq. 3 is rewritten as (Draper and Smith, 1966)

$$|X|^T\,|W|^{-1}\,|X|\,|b| = |X|^T\,|W|^{-1}\,|Z| \quad (5)$$

where $|b|$ is the estimated vector for $|\beta|$ which would minimize the sum of the matrix squared errors, $|E|^T \cdot |E|$, and $|W|$ is the weighting function matrix defined by:

$$|W|^{-1} = \begin{bmatrix} \frac{1}{\sigma_1^2} & & \bigcirc \\ & \frac{1}{\sigma_2^2} & \\ & & \ddots \\ \bigcirc & & \frac{1}{\sigma_n^2} \end{bmatrix} \quad (5a)$$

A simple empirical relation was assumed for σ:

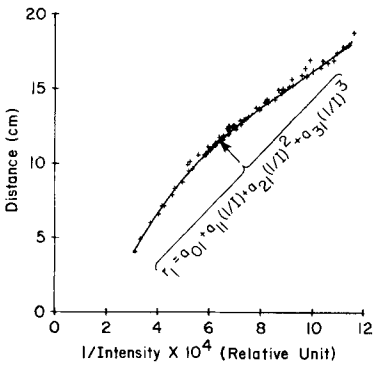

Figure 4. Typical in-situ calibration curve.

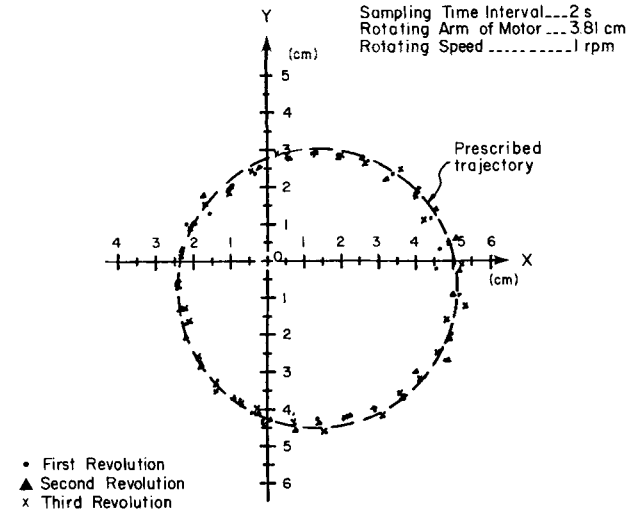

Figure 5. Comparison of measured instantaneous locations of a moving particle with its prescribed trajectory.

$$\sigma_i = \text{constant} \times r_i^m \tag{5b}$$

and, by trial and error, it was found that $m = 3$ would minimize the mean of $|\mu - \xi^2 - \eta^2 - \zeta^2|/\mu$ to our satisfaction. The tracer location is given by the solution vector $|b|$ which can be formally represented by:

$$|b| = (|X|^T |W|^{-1} |X|)^{-1} |X|^T |W|^{-1} |Z| \tag{6}$$

Sample Calibration Results

To assess the capability of the present facility, a prescribed circular trajectory of the tracer was provided by having it mounted at the tip of a rotating arm in the bed and driven by a synchronous motor. Only four detectors were used in this test, which was performed during the early stages of the research. A comparison of the measured instantaneous locations of the moving tracer with its prescribed trajectory is shown in Figure 5. The spatial resolution for individual position measurements was about 2 mm at a sampling interval of 2 seconds. Improved resolution has subsequently been obtained.

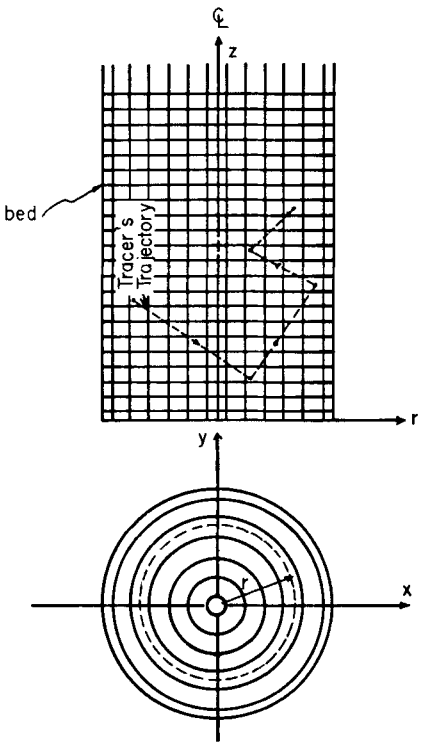

Figure 6. Sampling compartments used to calculate mean velocities and Lagrangian autocorrelations: 7 compartments in radial direction, 22 in axial direction.

Calculation of Mean Velocity Distribution

Instantaneous solids velocities were obtained by differentiating two successive locations at known data sampling rate. For the purpose of determining the mean velocity distribution, the bed was divided into 154 (i.e., 7 × 22) sampling compartments as shown in Figure 6. It should be noted that the azimuthal dependence of the solids velocity was found to be small and thus the average was taken over the entire 360 degrees despite the capability of the present techniques for measuring three-dimensional motion. By running experiments for sufficiently long durations, the repeated appearance of the tracer in a given compartment enables the ensemble-average of the instantaneous velocities to be calculated. For a typical running time of 2 hours using a sampling interval of 30 milliseconds, a total of 240,000 data points were obtained for an experiment. Since the probability of the tracer's occurrence in each compartment varies from compartment to compartment, the confidence level of ensemble-averaged data varies accordingly.

RESULTS AND DISCUSSION

Effects of Fluidizing Velocity on Particle Circulation Pattern

A number of experiments were conducted with the superficial air velocity, U_o, ranging from 32 to 89 cm/s. The corresponding ratio U_o/U_{mf} ranged from 1.65 to 4.60. It was found that the bed exhibited a variety of circulation flow patterns, being dependent strongly on the gas flow rate. Distributions of the solids mean velocity are summarily presented in Figure 7a–d for glass beads of diameters in the range of 0.42–0.6 mm. In these figures and others which follow, the starting point of the vector denotes the location in question; it also represents the center of the sampling compartment.

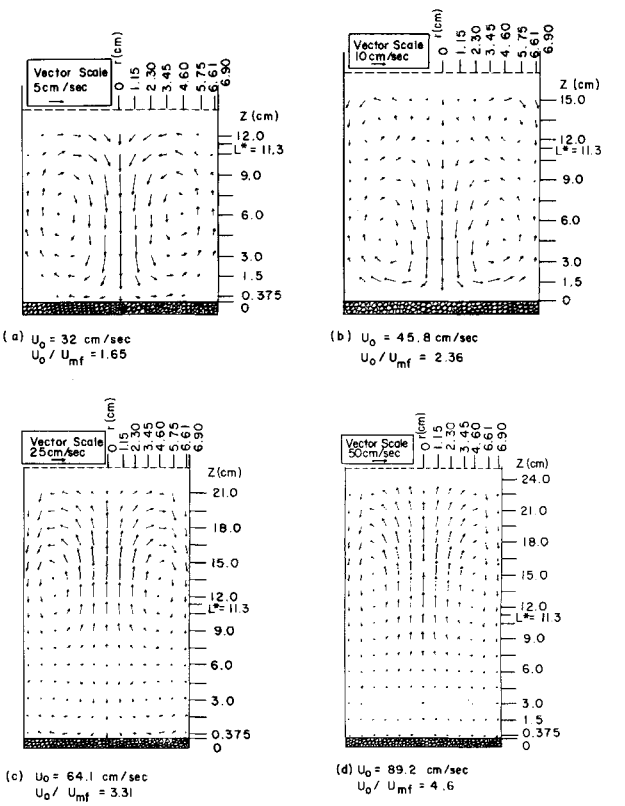

Figure 7. Particle circulation patterns at various fluidizing velocities for a gas fluidized bed of 0.42–0.6mm dia. glass beads; L^* denotes static bed height.

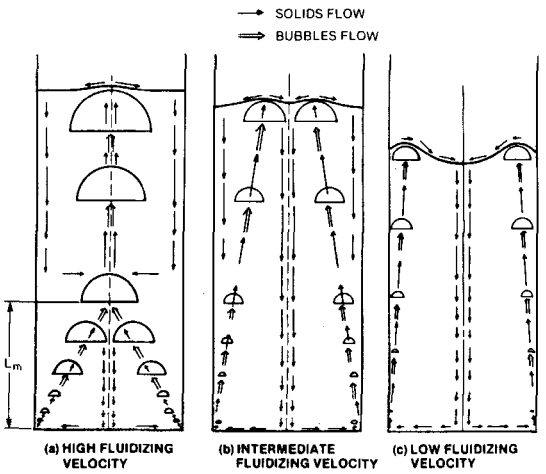

Figure 8. Development of solids recirculation due to bubble motion at various fluidizing velocities.

At the lowest fluidization velocity, the basic mean circulatory pattern of solids was that of a toroidal vortex ascending near the wall and descending at the center (AWDC) as shown in Figure 7a. As the gas velocity increased, a second toroidal vortex in the reverse direction—ascending at the center and descending near the wall (ACDW)—appeared in the upper portion of the bed although solids at the center remained flowing downward, Figure 7b. As the gas flow was further increased, the extent of the ACDW vortex grew while that of the AWDC diminished, Figure 7c, and eventually only the ACDW vortex existed in the bed, Figure 7d. It is of interest to note that for the experimental conditions of Figures 7c and 7d, there existed a narrow region between the two vortices where the solids movement was very weak or near stagnation. This narrow region or layer was occasionally visible as a stagnant ring on the cylindrical wall of the bed.

Similar trends were also observed for glass beads of 0.6–0.8 mm dia. (Lin, 1981).

The phenomena described in the foregoing paragraphs can be interpreted in terms of the bubble behavior. Werther and Molerus (1973) reported that close to the distributor plate intensified bubble activity existed in an annular region near the wall. As the bubbles detach and rise, they tend to move toward the center with increasing height. If the bed is sufficiently deep, they would eventually merge at the center. Whitehead et al. (1976) also observed that close to a uniform distributor bubbles formed preferentially near the wall of a large bed (1.2 m × 1.2 m vessel) because of the inherent pressure maldistribution near the distributor. Since the solids are carried upward in the wake of the bubbles, besides the drift of particles in the proximity of bubbles, they basically move along the bubble tracks. The downward motion of the solids ensues to maintain continuity.

In light of the presently measured solids recirculation patterns and the known bubble flow behavior, a schematic representation of their relationship is proposed and is illustrated in Figure 8a–c. The figures are, to a large extent, self-explanatory. At high fluidizing velocities, the bubbles would merge in the central region of the bed. This suggests that the phenomenon can be characterized by a length, L_m, the bubble merging height. In general, L_m is a function of the superficial gas velocity, particle size, particle density, bed diameter, and related factors. It may be reasoned that the simultaneous existence of both upward and downward solids flow in the central region would occur if $(L_m/L_f) < 1$, L_f being the expanded bed height. Werther and Molerus (1973) proposed similar pictorial presentation as that shown in Figure 8a–c, except that attention was directed to the influence of bed height instead of fluidizing velocity.

Solids Flow as Influenced by Nonuniform Distributor Plate

The configuration of the gas distributor plate plays a key role in bubble development, which in turn determines the flow patterns

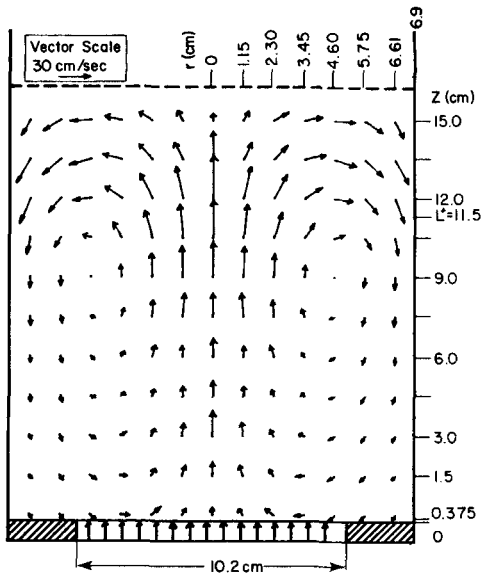

Figure 9. Velocity distribution for a bed of 0.6–0.8 mm glass beads fluidized with a nonuniform distributor plate: U_o = 63.1 cm/sec; L^* denotes static bed height.

of solids. Experiments were therefore conducted with a distributor plate that restricted the air flow to its central region, as illustrated in Figure 9. The ACDW vortex was intensified to such an extent that the AWDC vortex disappeared completely. Figure 9 also indicates the existence of a low velocity region near the corners adjacent to the distributor plate.

Solids Flow in the Presence of a Sphere

A very complex solids flow pattern was revealed when a solid sphere of 6 cm dia. was placed near the center of the expanded bed with a uniform distributor plate. As shown in Figure 10, there is a weak AWDC toroidal vortex in the region below the sphere. In the region where the blockage effect is most pronounced, there exists a toroidal vortex with strong upward motion in the neighborhood of the sphere and downward flow near the wall. Farther above, there are two additional vortices, one with a descending motion close to the surface of the supporting rod, another with descending motion close to the container wall. Comparing the

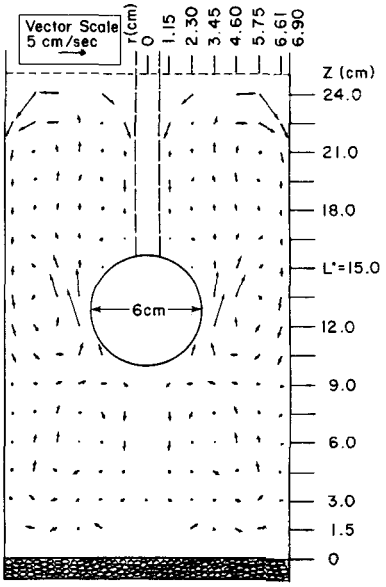

Figure 10. Velocity distribution for a fluidized bed of 0.42–0.6 mm glass beads with an immersed sphere: U_o = 47.8 cm/s; U_o/U_{mf} = 2.45; L^* denotes static bed height; sampling period 40 min.

TABLE 1. DEVIATIONS OF MASS FLOW BALANCE ACROSS A GIVEN SURFACE IN THE BED

Cylindrical Surface, cm	Deviation, % $\frac{\lvert\dot{M}_{in} - \dot{M}_{out}\rvert}{\frac{1}{2}(\dot{M}_{in} + \dot{M}_{out})}$
$r = 1.15$	2.2
$r = 2.30$	9.6
$r = 3.45$	2.3
$r = 4.60$	17.8
$r = 5.75$	6.2
$r = 6.61$	6.0
Horizontal Surface, cm	**Deviation %**
$z = 0.38$	8.7
$z = 1.5$	1.3
$z = 3.0$	3.3
$z = 4.5$	7.7
$z = 7.5$	7.9
$z = 9.0$	8.9
$z = 10.5$	0.0
$z = 12.0$	0.8
$z = 13.5$	1.4
$z = 15.0$	4.0
$z = 16.5$	10.2
$z = 18.0$	13.2

magnitudes of the velocity vector with those of Figure 7b, which is for a slightly lower U_o, one sees that the bulk circulation rate is significantly less. The appearance of the rather abrupt changes in the direction of solids motion at adjoining locations is due to the insufficient time spent in data collection.

Continuity Check for Solids Flow

It is believed that the number density of the tracer's occurrences in a sampling compartment can be interpreted as the solids volume fraction if the total number of data collected is sufficiently large. The number density distribution has been presented (Lin, 1981). The degree to which the conservation of mass is satisfied by the measured solids velocity distribution and the volume fraction distribution of solid phase can be used as a check of their accuracy. To carry out such a continuity check, a number of imaginary cylindrical surfaces with various radii extending from the distributor plate to a height where negligible particle motion exists, and a number of imaginary horizontal surfaces at various heights were selected for the calculation of mass flow rate. To satisfy the continuity equation, the net mass flow rate across each surface should be equal to zero. Hence, the difference between the average of the incoming mass flow rate ($\dot{M}_{in}$) and the outgoing mass flow rate ($\dot{M}_{out}$) provides a check on the overall accuracy of our measurements. The results of the calculation, carried out for the operating condition identical to that shown in the data for Figure 7c, are summarized in Table 1. The results indicate that the measured velocity distribution was reasonably consistent with the volume fraction distribution.

The area-averaged axial distribution of solids density was also calculated by counting the total number of tracer occurrences in a horizontal plane at various heights above the distributor plate. The results are shown in Figure 11. It is seen that the solids density in the neighborhood of boundary between the AWDC and ACDW vortices is relatively constant. As expected, an exponential decay of the density with increasing height is revealed in the ACDW recirculating region. However, the reverse trend is seen in the AWDC recirculating region.

Lagrangian Autocorrelation of Fluctuating Velocities

To develop some feeling about the statistical behavior of the particle motion, Lagrangian autocorrelation of the fluctuating velocities has been evaluated.

The Lagrangian autocorrelation coefficient $R_{\alpha\alpha}(\mathbf{x},\tau)$ at a given position $\mathbf{x}$ is defined by: (Tennekes and Lumley, 1972)

$$R_{\alpha\alpha}(\mathbf{x},\tau) = \frac{\langle v'_\alpha(\mathbf{a},t)\, v'_\alpha(\mathbf{a},t+\tau)\rangle}{\langle v'^2_\alpha(\mathbf{a},t)\rangle} \tag{7}$$

where v'_α is the fluctuating velocity in either axial ($\alpha = z$) or radial ($\alpha = r$) direction and $\mathbf{a}$ denotes the initial position of the particle which, in the present instance, is the tracer. The ensemble average (denoted by $\langle\ \rangle$ in Eq. 7) for $R_{\alpha\alpha}$ at any given location is determined in the following way. The event of interest is initiated each time the tracer is found in the sampling compartment at that location. Its fluctuating velocity and that at later times are computed. The event is considered to be reinitiated when the tracer is again found in the same compartment. To insure that the two sequences of data are statistically independent, the interval between the two succeeding starting times must be greater than a preset limit. This limit is equal to or greater than the time lag for which the Lagrangian autocorrelation becomes negligible.

Figure 12 shows some sample results for the axial autocorrelation coefficient R_{zz} at four axial locations not far from the centerline. The operating conditions were the same as those given in Figure 7c. It is seen that the axial motions near the distributor plate are essentially uncorrelated after a short time lag of a few hundredths of a second (corresponding to a distance of the order of 0.3 mm). At $z = 6$ cm, which roughly corresponds to the region separating the ACDW and AWDC vortices, the particles exhibit the longest memory. For greater values of z, the axial autocorrelation curves cross the zero axis again at shorter times. It is estimated that the frequency of particle random motion ranged from 1.6 Hz in the

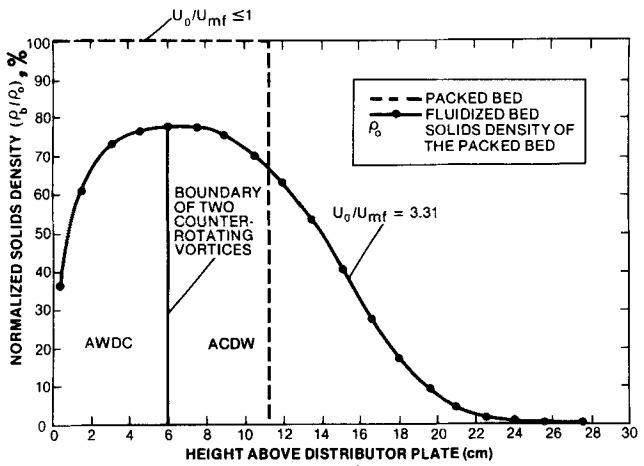

Figure 11. Area-averaged axial solids density distribution; conditions identical to Figure 7c.

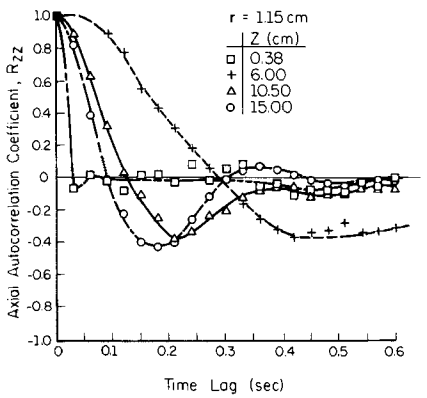

Figure 12. Typical values of axial autocorrelation at various locations; conditions identical to Figure 7c.

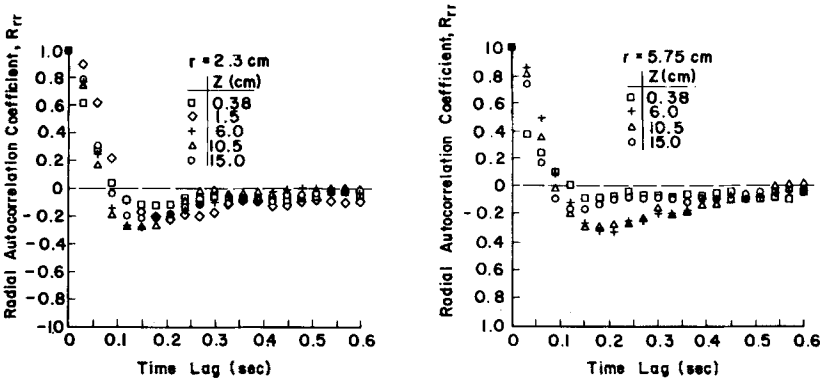

Figure 13. Typical values of radial autocorrelation at various locations; conditions identical to Figure 7c.

relatively stagnant layer to 16 Hz near the distributor plate while the frequencies in the ACDW vortex varied within a much narrow range (about 3.8–5 Hz).

It had been observed that in shallow beds the development of bubbles was accompanied with pressure fluctuations. Statistical analysis of the fluctuating pressure close to the distributor plate revealed that there existed simple harmonic oscillation (Lirag and Littman, 1971; Verloop and Heertjes, 1974). The frequency of the harmonic oscillation decreased with increasing bed height. For a 6.5 cm-ID bed containing 0.37 and 0.85 mm glass beads, the frequency measured at 3 mm above the distributor varied from 25 to 1 Hz for beds from 0.5 to 40 cm in depth (Verloop and Heertjes, 1974). The frequency range of pressure fluctuations appears to be in agreement with the present results.

The autocorrelation coefficients for the radial fluctuating velocities are shown in Figure 13. It is rather surprising to find that the variations of R_{rr} are remarkably insensitive to both radial and axial locations. More work needs to be done to understand the phenomenon.

ACKNOWLEDGMENT

Financial support provided by National Science Foundation under NSFENG 78-11115, by the Research Board of the University of Illinois, and by the Department of Energy under DE-FG22-81PC40804 is gratefully acknowledged.

NOTATION

$\mathbf{a}$ = vector of initial position of tracer
$|b|$ = matrix of least square estimated value for tracer coordinates
$|E|$ = error matrix
I = intensity of detected gamma ray
$\dot{M}_{in}$ = solids mass flow rate in negative direction
$\dot{M}_{out}$ = solids mass flow rate in positive direction
n = number of detectors
r_i = measured distance of tracer by ith detector
R = Lagrangian autocorrelation
U_{mf} = minimum fluidizing velocity
U_0 = superficial gas velocity
v' = particle fluctuating velocity
$|W|$ = weighting function matrix
$\mathbf{x}$ = position vector, locates center of compartment
x_i,y_i,z_i = coordinates of fictitious center of ith detector
$|X|$ = matrix of coordinates of effective centers of all n detectors
z = height from distributor plate
$|Z|$ = matrix of distances measured by detectors and of coordinates of fictitious centers of detectors

Greek Letters

ξ,η,ζ = coordinates of tracer location to be determined
μ $\equiv \xi^2 + \eta^2 + \zeta^2$
$|\beta|$ = matrix of coordinates of tracer
ϵ_i = estimating error associated with ith detector
σ_i = variance associated with measurement by ith detector
τ = time lag
ρ_b = solids density of fluidized bed
ρ_o = solids density of packed bed

Subscripts

i = ith detector
r = radial component
z = axial component
α = either r or z component

Symbols

$\langle\ \rangle$ = ensemble average

LITERATURE CITED

Carlos, C. R., and J. F. Richardson, "Solids Movement in Liquid Fluidized Beds. 1: Particle Velocity Distribution," *Chem. Eng. Sci.*, **23**, 813 (1968).

Draper, N. R., and H. Smith, *Applied Regression Analysis*, John Wiley & Sons, New York (1966).

Handley, D. A., et al., "A Study of the Fluid and Particle Mechanics in Liquid Fluidized Beds," *Trans. Inst. Chem. Eng.*, **44**, T260 (1966).

Kmiec, A., "Particle Distributions and Dynamics of Particle Movement in Solid-Liquid Fluidized Beds," *Chem. Eng. J.*, **15**, 1 (1978).

Kondukov, et al., "An Investigation of the Parameters of Moving Particles in a Fluidized Bed by a Radioisotropic Method," *Int. Chem. Eng.*, **4**, 43 (1964).

Latif, B. A. J., and J. F. Richardson, "Circulation Patterns and Velocity Distributions for Particles in a Liquid Fluidized Bed," *Chem. Eng. Sci.*, **27**, 1933 (1972).

Leva, *Proc. Symp. on Interaction between Fluids and Particles*, 143, Inst. Chem. Engineers, London (1962).

Lin, J. S., "Particle-Tracking Studies for Solids Motion in a Gas Fluidized Bed," Ph.D. Thesis, Univ. Illinois, Urbana-Champaign (1981).

Lirag, R. C., and H. Littman, "Statistical Study of the Pressure Fluctuations in a Fluidized Bed," *AIChE Symp. Ser.*, **67** (116), 11 (1971).

Marsheck, R. M., and A. Gomezplata, "Particle Flow Patterns in a Fluidized Bed," *AIChE J.*, **11**, 167 (1965).

Massimilla, L., and J. W. Westwater, "Photographic Study of Solid-Gas Fluidization," *AIChE J.*, **6**, 134 (Jan., 1960).

Merry, J. M. D., and J. F. Davidson, " 'Gulf Stream' Circulation in Shallow Fluidized Beds," *Trans. Inst. Chem. Eng.*, **51**, 361 (1973).

Ohki, K., and T. Shirai, "Particle Velocity in Fluidized Bed," *Fluidization Tech.*, D. Keairns, Ed., **1**, 95, McGraw-Hill (1975).

Oki, K., W. P. Walawender, and L. T. Fan, "The Measurement of Local Velocity of Solid Particles," *Powder Tech.*, **18**, 171 (1977).
Oki, K., M. Ishida, and T. Shirai, "The Behavior of Jets and Particles near the Gas Distributor Grid in a Three-Dimensional Fluidized Bed," *Proc. Int. Conf. Fluidization*, 421, Henniker, New Hampshire, (1980).
Tennekes, H., and J. L. Lumley, *A First Course in Turbulence*, 224, MIT Press, Cambridge, MA (1972).
Velzen, D. V., et al., "Motion of Solids in Spouted Beds," *Can. J. Chem. Eng.*, **52**, 156 (1974).
Verloop, J., and P. M. Heertjes, "Periodic Pressure Fluctuations in Fluidized Bed," *Chem. Eng. Sci.*, **29**, 1035 (1974).
Werther, J., and O. Molerus, "The Local Structure of Gas Fluidized Beds. II: The Spatial Distribution of Bubbles," *Int. J. Multiphase Flow*, **1**, 123 (1973).
Whitehead, A. B., G. Gartside, and D. C. Dent, "Fluidization Studies in Large Gas-Solid Systems. III: The Effect of Bed Depth and Fluidizing Velocity on Solids Circulation Patterns," *Powder Technol.*, **14**, 61 (1976).

Manuscript received Feb. 16, 1983; revision received Oct. 31, 1983, and accepted Nov. 11.

Transport Processes in Narrow (Capillary) Channels

Rates of mass and momentum transport in narrow flow channels (gaps 0.2–0.5 mm) have been determined over a wide range of flow velocities, 220–7,700 cm/sec (Re 1,300 to 22,000). Existing correlations that apply to smooth channels of much larger hydraulic diameter were found to be valid for the narrow channels as well. However, in the turbulent regime the condition of hydraulic smoothness could be satisfied only when the walls were optically smooth. Transport rates to rough walls were also measured. The ratio of the mass transport to the momentum transport in the form of $j_D/(f/2)$—a measure of the improved mass transfer compared to the increased pressure drop—is given for the smooth and rough-wall cells over the Re range studied.

R. E. ACOSTA,
R. H. MULLER,
and C. W. TOBIAS

Lawrence Berkeley Laboratory
University of California, Berkeley
Berkeley, CA 94720

SCOPE

The use of very thin channels for the purpose of heat or mass transfer is becoming widespread for a number of applications, including nuclear reactors, electrochemical machining, and electro-organic syntheses. Empirical correlations available to calculate rates of momentum and mass transport in the turbulent regime have been obtained using flow channels with an equivalent diameter of 2 cm or more. In the present work the applicability of these correlations to mass transfer in very thin channels (fractions of a millimeter) was tested. Because of the very large pressure drops involved in processes using very thin channels, the expenditure in pumping power becomes an important economic consideration. Accordingly, the conditions under which maximum mass transfer (or heat dissipation) may be achieved with a minimum pressure drop were also studied. Rates of mass transfer were determined using an electrochemical technique: measurement of limiting currents. The rates of momentum transport were determined by measuring the pressure drop in the same channels where the mass transport rates were measured. For the very small hydraulic diameters employed in this work it was found that the condition of hydraulic smoothness could be satisfied only when the walls of the channel were optically smooth. Because in practical situations the latter condition is seldom found, four degrees of roughness were employed in addition to smooth walls.

CONCLUSIONS AND SIGNIFICANCE

Coefficients for mass and momentum transport in rectangular cross-sectional channels with equivalent diameters of 0.096 and 0.038 cm have been successfully determined in the Reynolds number range of 1,300 to 22,000. At the largest Reynolds numbers employed, an equivalent mass transfer boundary-layer thickness of 2.3×10^{-5} cm was obtained. Mass transfer boundary layers as thin as this do not appear to have been previously reported for channel flows.

The coefficients of mass and momentum transport in smooth rectangular channels with wall separations in the range of fractions of a millimeter can successfully be correlated by the equations that apply to smooth channels of much larger equivalent diameter. However, for thin channels to be considered hydraulically smooth at $Re \geq 2{,}500$, the walls must be polished to optical smoothness. Since this condition is rarely encountered in practical applications, care must be exercised in extrapolating results obtained with large equivalent diameter channels.

Under conditions where the Reynolds number falls in the laminar regime, only very gross surface roughness has an effect on the value of the transport coefficients. For smooth surfaces the mass transfer rate is given by the extension to the Graetz-Leveque solution:

$$Sh_{ave} = 1.85\,(ReScD_h/x)^{1/3}$$

Correspondence concerning this paper should be addressed to R. E. Acosta. Present address: IBM T. J. Watson Research Center, P.O. Box 218, Yorktown Heights, NY 10598.